

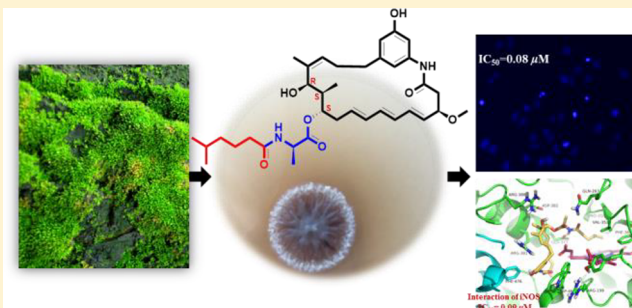
Ansamycins with Antiproliferative and Antineuroinflammatory Activity from Moss-Soil-Derived *Streptomyces cacaoi* subsp. *asoensis* H2S5

Dan Tang,[†] Ling-Li Liu,[†] Qiu-Rui He, Wen Yan, Ding Li, and Jin-Ming Gao^{*✉}

Shaanxi Key Laboratory of Natural Products & Chemical Biology, College of Chemistry & Pharmacy, Northwest A&F University, Yangling 712100, Shaanxi, People's Republic of China

Supporting Information

ABSTRACT: Three new 21-membered macrocyclic benzenoid ansamycins, trienomycins J–L (1–3), together with seven known analogues, trienomycins A–G (4–10), were isolated from liquid culture of the moss soil-derived actinomycete *Streptomyces cacaoi* subsp. *asoensis* H2S5. The structures of the new compounds were elucidated by extensive NMR spectroscopic analysis and HRESIMS data. The absolute configurations of trienomycins were established by Marfey's method. Antiproliferative assays showed that compound 1 had the greatest activity against HepG2 cells, with an IC_{50} value of 0.1 μ M. The induction of apoptosis of HepG2 cells by 1 was investigated by flow cytometry and evaluation of nuclear morphology. In addition, all of the compounds inhibited nitric oxide production with IC_{50} values of 0.02 to 8.3 μ M, and compounds 1, 4, and 7 were the most potent inhibitors. These findings will facilitate the development of new antineuroinflammatory agents.



Ansamycins, which are characterized by a macrocyclic lactam structure, are microbial metabolites with cytotoxic, antibacterial, and anti-inflammatory activities.^{1–3} The biosynthesis of ansamycins involves a 3-amino-5-hydroxybenzoic acid (AHBA) starter unit and type I modular polyketide synthesis.^{4,5} The first group of ansamycins isolated was the rifamycins, which exhibited broad-spectrum antibacterial activity.^{6,7} A second important group of ansamycins are the trienomycins, which are distinguished by their 21-membered macrolactam and a carboxylic acid moiety attached via a D-alanine residue to the polyketide backbone.^{8–11} To date, more than 50 trienomycins with diverse bioactivities have been reported.^{12–14} For example, trienomycin A is a potent cytotoxic agent that is considerably less toxic to non-transformed cells.¹ Structure–activity relationship (SAR) studies of trienomycin A showed that its bioactivity is dependent on the acyl chain attached at C-11, the triene motif, and the hydroxy group at C-13.^{15,16} The unusual structure and promising bioactivity of trienomycins have resulted in synthetic^{17,18} and biosynthetic studies.^{19,20} However, libraries of compounds with greater structural diversity are needed for optimal drug discovery and development.

As part of our ongoing research on bioactive molecules from microorganisms,^{21–24} we isolated strain H2S5, which was identified by 16S rRNA gene sequence analysis as *Streptomyces cacaoi* subsp. *asoensis*, from moss soil collected on the north slope of Taibai Mountain in northwest China. The genome of

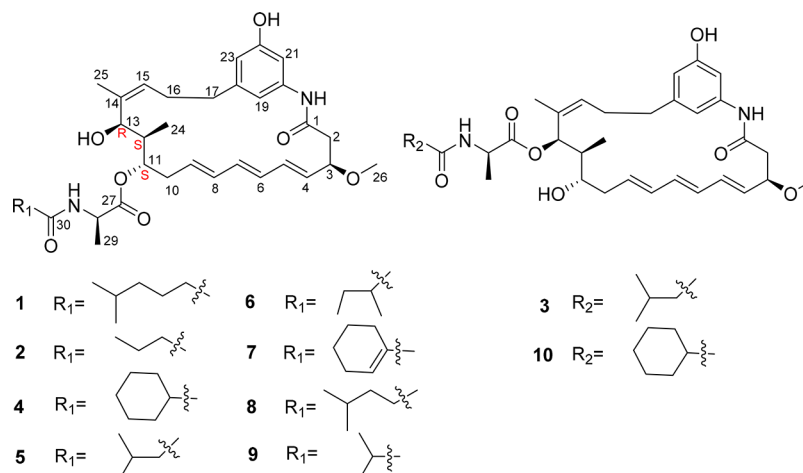
S. cacaoi subsp. *asoensis* H2S5 was sequenced using massively parallel sequencing (MPS) Illumina technology and assembled by SOAPdenovo.^{25,26} The whole genome sequence was submitted to antiSMASH bioinformatics software for secondary metabolite pathway analysis.²⁷ The identification of a gene cluster containing a type I PKS and AHBA-related genes resulted in further investigation of this bacterium, revealing its production of compounds with a unique UV absorption pattern. Subsequent large-scale fermentation and repeated chromatography steps led to the isolation of 10 trienomycin analogues (1–10) including three new compounds (1–3). We report here the isolation and structural and functional characterization of these compounds.

RESULTS AND DISCUSSION

Trienomycin J (1) was isolated as a white powder. The molecular formula $C_{36}H_{52}N_2O_7$ was determined by HRESIMS. The UV spectrum of 1 revealed absorption maxima at 250, 260, 271, and 282 nm, indicating a conjugated moiety. The 1H , ^{13}C , and HSQC NMR data (Table 1) displayed a 1,3,5-trisubstituted benzene ring due to three singlets at δ_H 6.43 (H-19), 7.00 (H-21), and 6.39 (H-23) and conjugated triene signals at δ_H 6.08–6.16 (4H, m, H-5, H-6, H-7 and H-8) and δ_H 5.57–5.63 (2H, m, H-4, H-9). In addition to these

Received: March 9, 2018

Chart 1

Table 1. ¹H and ¹³C NMR Spectroscopic Data for Compounds 1, 2, and 3

position	1		2		3	
	δ_C , type	δ_H (J in Hz)	δ_C , type	δ_H (J in Hz)	δ_C , type	δ_H (J in Hz)
1	171.9, C		170.9, C		170.9, C	
2	44.8, CH ₂	2.44/2.72, m	44.8, CH ₂	2.42/2.74, m	44.8, CH ₂	2.41/2.73, m
3	81.6, CH	4.05, m	81.6, CH	4.06, m	81.7, CH	4.08, m
4	131.1, CH	5.60, m	130.4, CH	5.60, m	132.3, CH	5.56, m
5	132.6, CH	6.11, m	131.0, CH	6.18, m	130.6, CH	6.12, m
6	130.4, CH	6.09, m	134.7, CH	6.18, m	134.2, CH	6.12, m
7	135.2, CH	6.14, m	135.2, CH	6.14, m	135.0, CH	6.13, m
8	134.9, CH	6.15, m	135.0, CH	6.15, m	134.7, CH	6.09, m
9	134.7, CH	5.60, m	132.5, CH	5.60, m	131.8, CH	5.75, m
10	33.5, CH ₂	2.31/2.53, m	33.7, CH ₂	2.30/2.52, m	37.4, CH ₂	2.30/2.42, m
11	76.4, CH	4.84, m	76.5, CH	4.84, m	72.0, CH	3.64, m
12	40.5, CH	1.95, m	40.5, CH	1.95, m	41.4, CH	1.97, m
13	69.7, CH	4.62, br s	69.7, CH	4.64, br s	75.4, CH	5.87, d (5.5)
14	139.7, C		139.7, C		135.4, C	
15	125.9, CH	5.22, m	126.0, CH	5.23, m	128.6, CH	5.33, m
16	30.3, CH ₂	1.98/2.28, m	30.6, CH ₂	1.96/2.27, m	30.7, CH ₂	1.97/2.40, m
17	37.3, CH ₂	2.44, m	37.3, CH ₂	2.43, m	37.1, CH ₂	2.49, m
18	144.9, C		145.0, C		144.9, C	
19	113.4, CH	6.43, s	113.3, CH	6.43, s	113.4, CH	6.48, s
20	140.2, C		140.2, C		140.2, C	
21	107.1, CH	7.00, br s	107.1, CH	7.01, br s	107.1, CH	6.97, br s
22	158.7, C		158.7, C		158.6, C	
23	112.8, CH	6.39, s	112.7, CH	6.40, s	112.9, CH	6.42, s
24	10.1, CH ₃	0.93, m	10.1, CH ₃	0.91, m	10.7, CH ₃	0.94, d (6.9)
25	20.7, CH ₃	1.75, s	20.7, CH ₃	1.75, s	20.6, CH ₃	1.68, s
26	56.7, OCH ₃	3.32, s	56.6, OCH ₃	3.32, s	56.6, OCH ₃	3.32, s
27	173.7, C		173.7, C		173.9, C	
28	50.0, CH	4.31, m	50.0, CH	4.33, m	49.7, CH	4.41, m
29	17.2, CH ₃	1.36, d (7.3)	17.2, CH ₃	1.37, d (7.3)	17.4, CH ₃	1.41, d (7.3)
30	176.5, C		176.1, C		175.5, C	
31	35.4, CH ₂	2.22, m	38.5, CH ₂	2.16, m	45.9, CH ₂	2.10, m
32	34.4, CH ₂	1.36, m	20.2, CH ₂	1.53, m	27.4, CH	2.06, m
33	33.7, CH ₂	1.41/1.64, m	14.0, CH ₃	0.93, m	22.7, CH ₃	0.98, d (6.2)
34	30.5, CH	1.18/1.38, m			22.8, CH ₃	0.99, d (6.2)
35	11.6, CH ₃	0.89, m				
36	19.4, CH ₃	0.90, m				

resonances, a methoxy singlet at δ_H 3.32 (H-26) and five methyl groups at δ_H 1.75 (s, H₃-25), 1.36 (d, $J = 7.3$, H₃-29), and 0.89–0.93 (9H, m, H₃-24, H₃-35, H₃-36) were observed.

The above information was in good agreement with the data reported for trienomycin A, suggesting that compound 1 shared the same *ansa* ring and alanine moiety as trienomycin

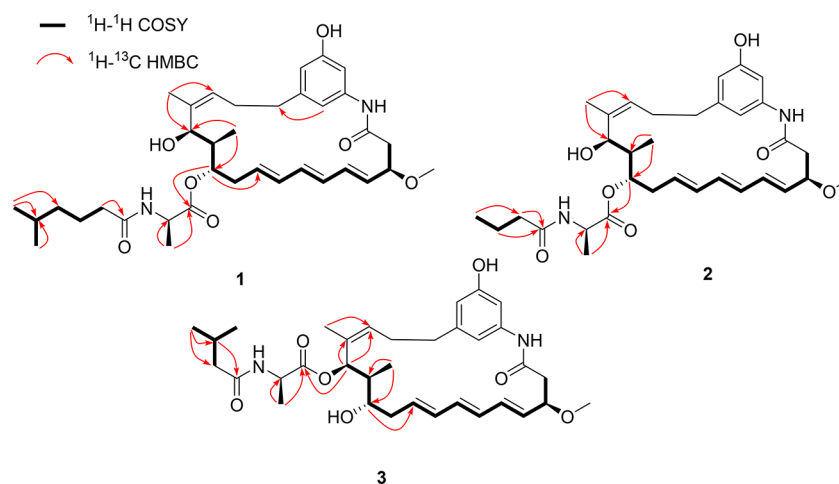


Figure 1. Key COSY and HMBC correlations of compounds **1**, **2**, and **3**.

A. The ^1H – ^1H COSY correlations of H-31/H-32/H-33/H-34/H-35/H-36 and the HMBC correlations (Figure 1) of the methyl groups H-35 and H-36 with C-34, and a methylene at δ_{H} 2.22 (2H, m, H-31) to C-30 (δ_{C} 176.5), indicated that an isohexyl group was anchored at the 27-alanine through an amide linkage. The remaining structure of **1** was confirmed by the ^1H – ^1H COSY correlations of H-2/H-3/H-4/H-5/H-6/H-7/H-8/H-9/H-10/H-11/H-12/H-13 and the HMBC correlations of H₃-25/C-15, H₃-24/C-11, and H-11/C-27. Thus, the gross structure of **1** was determined as depicted.

Trienomycin K (**2**) was obtained as a white powder, which had the molecular formula $\text{C}_{33}\text{H}_{46}\text{N}_2\text{O}_7$ based on HRESIMS. The UV spectrum of **2** was similar to that of metabolite **1**. The ^1H and ^{13}C NMR spectral data of **2** (Table 1) were also similar to those of **1**, indicating that they have the same carbon skeleton. The main differences were the absence of methyl, methylene, and methenyl groups. Interpretation of the ^1H – ^1H COSY spectrum established a fragment consisting of three carbon units (Figure 1), which spanned from C-31 (δ_{C} 38.5) to C-33 (δ_{C} 14.0). This fragment was connected at C-30 (δ_{C} 176.1) based on the HMBC correlations of H-31 (δ_{H} 2.16)/C-30 and H-32 (δ_{H} 1.53)/C-30. On the basis of these data, the structure of **2** was determined as shown.

Trienomycin L (**3**) was purified as a white powder and determined to have a molecular formula of $\text{C}_{34}\text{H}_{48}\text{N}_2\text{O}_7$ based on HRESIMS. The molecular weight was identical to that of the co-isolated compound, trienomycin B (**5**), and the ^1H and ^{13}C NMR spectral data were similar to those of trienomycin B. In comparison with those of trienomycin B, the chemical shift of H-13 in compound **3** (Table 1) was shifted downfield to δ_{H} 5.87. The ^{13}C NMR chemical shift of C-11 in **3** was shifted upfield to δ_{C} 72.0 (δ_{C} 76.4 in trienomycin B), while that for C-13 was shifted downfield to δ_{C} 75.4 (δ_{C} 69.7 in trienomycin B). From these spectral data, it was speculated that the alanine moiety might be linked to C-13 in **3** instead of C-11 as in trienomycin B. The HMBC correlation (Figure 1) between H-13 (δ_{H} 5.87) and the carbonyl carbon C-27 (δ_{C} 173.9) confirmed the linkage position of the alanine moiety at C-13. Hence, the structure of **3** was determined. This is the second report of a trienomycin with an alanine moiety attached at the C-13 position, the first being reported by Yoo and co-workers.¹¹

Seven known compounds were also isolated from the extract and identified as trienomycins A–G (4–10), by comparing

their NMR data with those in the literature.^{8–11} The relative and absolute configurations of the ansamycin antibiotics (+)-trienomycins A–C (4–6) were elucidated by chemical synthesis.²⁸ In this study, we isolated sufficient compound **4** for absolute configuration analysis. The absolute configuration of alanine was assigned by comparing the retention time and mass data of the hydrolysis products of **4** (6 N HCl, 120 °C, 16 h) after derivatization with Marfey's reagent (1-fluoro-2,4-dinitrophenyl-5-L-leucineamide, L-FDLA) with those of D/L-alanine standards by HPLC-MS.²⁹ The results indicated that the absolute configuration of the amino acid residues was D-alanine (Figure S21 and Table S1).

To determine the relative and absolute configurations of C-11, -12, and -13 in trienomycins, the corresponding acetonide derivative was prepared.²⁸ Thus, the deacylation of **4** with LiAlH_4 , followed by acetonide formation, gave the derivative **11** (Scheme S1), established as $\text{C}_{29}\text{H}_{39}\text{NO}_5$ by HRESIMS. The ^1H NMR spectrum of **11** showed the signals for H-11 at δ_{H} 4.03 as a broad triplet ($J_{11,12} = 10.6$) and H-13 at δ_{H} 4.58 as a doublet ($J_{12,13} = 5.5$), indicating the opposite orientation of H-11 and H-12 and the same side of H-12 and H-13, consistent with the acetonide trienomycin A.²⁸ Furthermore, the optical rotation of **11** $\{[\alpha]_{\text{D}}^{24} +140$ (c 0.21, CHCl_3) $\}$ was in close agreement with the reported acetonide trienomycin A $\{[\alpha]_{\text{D}}^{24} +191$ (c 0.21, CHCl_3) $\}$. Thus, the absolute configuration of **4** was established as 11S, 12S, and 13R. All isolated trienomycins had the same macrolactam backbone with different side chains at the C-11 or C-13 position. Therefore, the relative and absolute configurations of the macrolactam backbone of the three new compounds **1–3** were in good agreement with those of **4**.

Trienomycins are cytotoxic to cancer cell lines,^{1,13} and so the cytotoxicity of the isolated compounds against two human cancer cell lines, PC-3 and HepG2, was evaluated using the sulforhodamine B (SRB) method, with doxorubicin as a positive control.³⁰ As shown in Table 2, all compounds displayed cytotoxicity. Compounds **4** and **7** showed greater cytotoxicity than the positive control against PC-3 cells. Compound **1** showed the greatest cytotoxicity against HepG2 cells (IC_{50} 0.1 μM) and so was used for further analyses.

Induction of apoptosis of cancer, but not normal, cells is a promising anticancer strategy. To investigate whether apoptotic cell death contributed to the **1**-induced cytotoxicity in HepG2 cells, a nuclear morphological evaluation study was

Table 2. Cytotoxic Activities of Compounds 1–10 against PC-3 and HepG2 Cells

compound	IC ₅₀ (μM)		compound	IC ₅₀ (μM)	
	PC-3	HepG2		PC-3	HepG2
1	2.7	0.1	7	0.7	0.2
2	4.5	3.0	8	4.2	0.2
3	11.9	20.5	9	4.4	0.4
4	0.4	0.2	10	10.2	17.6
5	4.5	1.0	doxorubicin	0.8	0.7
6	2.6	0.5			

conducted by fluorescence microscopy Hoechst staining. As shown in Figure 2, dimethyl sulfoxide (DMSO)-treated control

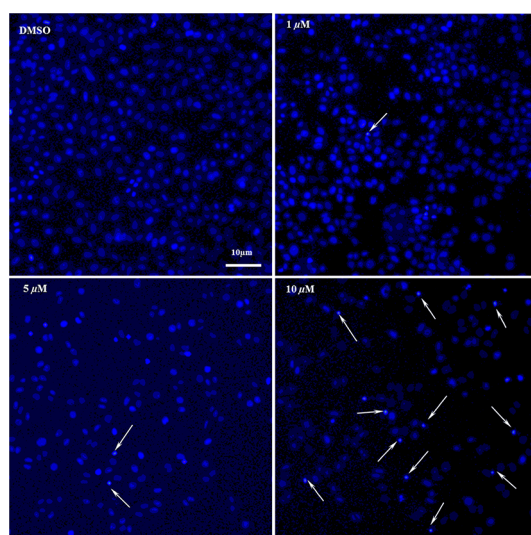


Figure 2. Morphological changes in HepG2 cells treated by **1** for 48 h. The apoptotic cells are indicated by white arrows.

cells had normal nuclei (blue stained and round). In contrast, HepG2 cells exposed to 5.0 and 10 μM compound **1** for 48 h exhibited chromatin condensation and cell shrinkage. These morphological changes of HepG2 cells supported the proapoptotic effect of **1**.

The apoptosis-inducing effect of **1** was confirmed by flow cytometric analysis. HepG2 cells were treated with 0.5, 1.0, and 5.0 μM **1** for 48 h, stained with annexin V–FITC and propidium iodide (PI), and analyzed by flow cytometry. Treatment with 0.5 μM compound **1** for 48 h resulted in frequencies of early and late apoptotic cells of 5.1% and 1.3%, respectively (Figure 3). Treatment with **1** at 1.0 and 5.0 μM increased the early and late apoptosis frequencies to 9.5% and 17.6%, and 1.7% and 5.7%, respectively.

To determine whether apoptosis was caused by cell-cycle arrest, the cell-cycle distribution of HepG2 cells treated with **1** was evaluated by flow cytometry. As shown in Figure 4, after treatment with 0.5, 1.0, or 5.0 μM **1** for 24 h, the percentages of HepG2 cells in S phase were 24.7%, 34.5%, and 38.6%, respectively, compared to 25.5% in control cells. Therefore, the apoptosis induced by **1** was related to cell-cycle arrest.

Neuroinflammation, due in part to uncontrolled microglial activation, may contribute to the pathogenesis of neurodegenerative diseases, such as Alzheimer disease (AD). Activated microglial cells in the central nervous system (CNS) produce inflammatory mediators such as nitric oxide

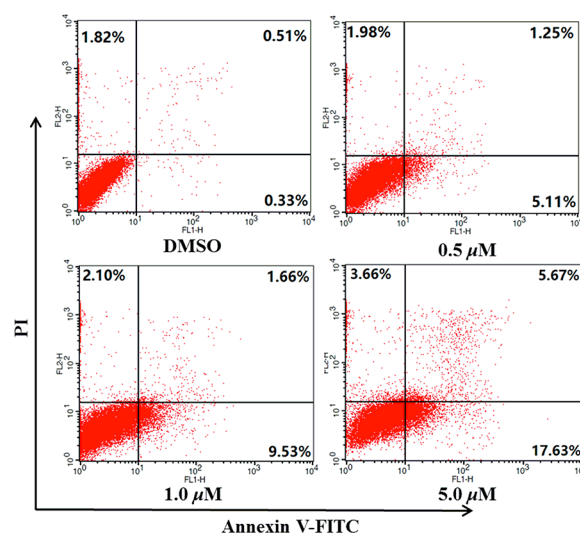


Figure 3. Apoptosis induced in HepG2 cells by **1**. Cells were treated for 48 h with the indicated concentrations of **1** followed by an annexin V–FITC and PI staining procedure. Lower right quadrants: percentage of early stage apoptotic cells; upper right quadrants: percentage of late-stage apoptotic cells; upper left quadrants: percentage of necrotic cells. Each experiment was performed in triplicate.

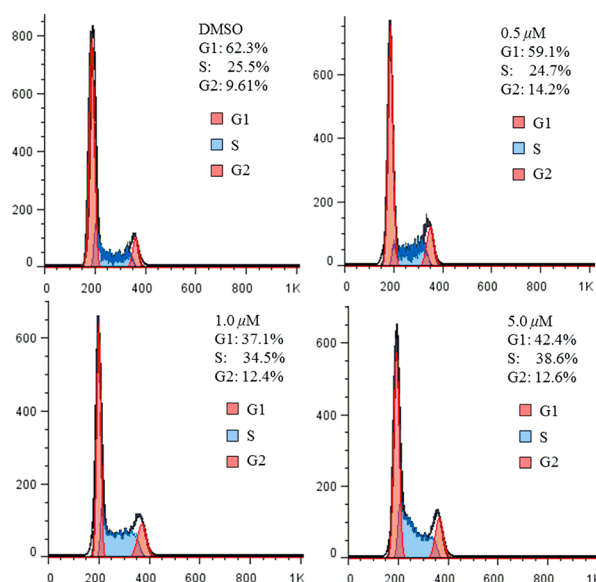


Figure 4. Effects of **1** on cell-cycle distribution in HepG2 cells. Cells were treated with the indicated concentrations of **1** for 24 h. Cellular DNA was stained with PI, and flow cytometry analysis was performed to determine cell-cycle distribution. Histograms show one representative example from three independent experiments.

(NO). Overproduction of NO in the CNS resulting from the production of inducible nitric oxide synthase (iNOS) can lead to uncontrolled neuroinflammation.²⁴ The inhibitory effect of the isolated compounds on lipopolysaccharide (LPS)-induced NO production in BV-2 microglial cells was assessed with quercetin as the positive control. Compounds **1**, **4**, and **7** showed high inhibitory activities (IC₅₀ 0.1, 0.02, and 0.03 μM, respectively; positive control IC₅₀ = 2.4 μM) (Table 3). The other compounds also exhibited significant inhibitory activity (IC₅₀ ≤ 10 μM). The compound with an *N*-cyclohexylcarbonyl group (**4**) was more active than the compound with an *N*-

Table 3. Inhibitory Effects of Compounds 1–10 on NO Production Induced by LPS in BV-2 Microglial Cells and Corresponding Binding Energy in Molecular Docking Studies

compound	IC ₅₀ (μM)	cell viability ^a (%)	binding energy (kcal/mol)
1	0.09 ± 0.01	83.8	−12.63
2	1.7 ± 0.2	96.0	−9.69
3	8.3 ± 0.7	83.1	−9.11
4	0.02 ± 0.01	95.2	−11.33
5	1.1 ± 0.1	92.7	−9.97
6	0.48 ± 0.01	76.3	−10.96
7	0.03 ± 0.01	94.3	−10.96
8	0.18 ± 0.01	82.5	−9.9
9	2.9 ± 0.4	85.4	−9.43
10	0.3 ± 0.1	93.1	−10.92
quercetin ^b	2.4 ± 0.7	99.2	^c

^aCell viability was expressed as a percentage (%) of that the LPS-only treatment group. ^bPositive control. ^cWas not conducted.

isohexylcarbonyl group. The length of the carboxylic acid moiety attached to the alanine residue also affected the activity of **1**, **2**, **5**, **6**, **8**, and **9**; a shorter aliphatic chain resulted in lower activity. The activity of compound **3**, which has an *N*-isobutyl *D*-Ala side chain at C-13 instead of C-11, was 7-fold lower than **5**. These data suggest that exposure of the 13-OH group increases activity. None of the 10 compounds showed cytotoxicity at the test concentrations. These preliminary structure–activity relationship results are consistent with previous reports.^{15,16}

To gain insight into the interactions between the compounds and proteins related to inhibition of NO, we performed molecular-docking analyses of the 10 compounds with iNOS (Figure S1, Supporting Information) as described previously.²⁴ The results were consistent with those of *in vitro* NO production assays (Figure S2, Supporting Information). Compounds **1**, **4**, and **7**, which exhibited high NO inhibitory activity, bound firmly to the catalytic site of iNOS (binding energy = −12.63, −11.33, and −10.96 kcal/mol, respectively; Table 3). The positions of compounds **1**, **4**, and **7** with respect to the key residues in the binding site are shown in Figure 5. The three compounds had similar binding modes. The phenol moiety was stacked against the aromatic rings of Trp463. Compounds with higher IC₅₀ values had higher binding energies, providing insight into the protein–ligand interactions. Taken together, the above results indicate that these compounds could be developed further as inhibitors of NO production.

EXPERIMENTAL SECTION

General Experimental Procedures. Optical rotations were acquired on an Autopol III automatic polarimeter (Rudolph Research Analytical). UV spectra were measured on a Shimadzu UV-1750 UV–vis spectrophotometer. IR spectra were recorded on a Bruker Tensor 27 FT-IR spectrometer with KBr pellets. 1D and 2D NMR spectra were obtained on a Bruker Avance III spectrometer (500 and 125 MHz for ¹H and ¹³C NMR, respectively) with tetramethylsilane as an internal standard. ESIMS was measured on an LTQ Fleet instrument (Thermo Fisher Scientific Inc., USA). HRESIMS data of new compounds were acquired on a Thermo Fisher Scientific Q-TOF mass spectrometer. The high-speed counter-current chromatography (HSCCC) system was composed of an OptiChrome-300 PLUS apparatus (OptiChrome, Jiangyin, China), a UV3000D metering pump, a UV3000 spectrometer, a BSZ-100 fraction collector (QTe,

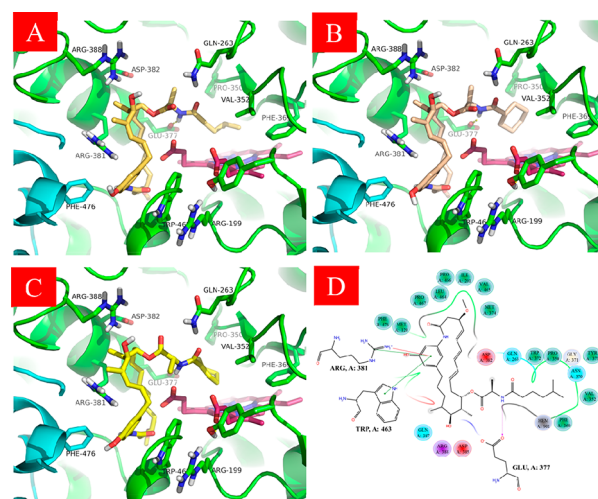


Figure 5. Molecular-docking simulations of **1** (A, khaki), **4** (B, tan), and **7** (C, yellow) into the iNOS binding site obtained in the lowest energy conformation. (D) Two-dimensional interaction map of the optimized docking model of **1** in the binding pocket of iNOS.

Shanghai, China), and CXTH-3000 ChemStation. HPLC analysis was performed on a Waters 1525 binary pump, coupled to a Waters 2489 detector (monitored wavelengths: 210 and 271 nm), equipped with a 4.6 mm × 250 mm, 5 μm, Hypersil BDS C₁₈ column. Semipreparative HPLC was achieved on a Shimadzu LC-20AP system, using a 10 mm × 250 mm, 5 μm, YMC C₁₈ column. Column chromatography (CC) was undertaken with silica gel (200–300 mesh, Qingdao Marine Chemical Ltd., China), RP-18 gel (20–45 μm, Fuji Silysia Chemical Ltd., Japan), or Sephadex LH-20 (40–70 μm, Amersham Pharmacia Biotech AB, Sweden). Fractions were monitored by thin-layer chromatography using silica GF254 (10–20 μm, Qingdao Marine Chemical Ltd., China). Flow cytometric analysis was performed on a FACS Calibur, Becton-Dickinson, San Jose, CA, USA. A total of 20 000 and 10 000 cells were acquired per sample for apoptosis and cell-cycle analysis, respectively, and data were analyzed using Cellquest software (Becton Dickinson).

Biological Material. Following standard procedures, an actinomycete was isolated from a moss soil sample collected from the northern slope of Taibai Mountain (33°57′–34°58′ N, 107°45′–107°53′ E), Shaanxi Province, China. It was identified as *Streptomyces cacaoi* subsp. *asoensis* H2S5 (GenBank accession no. KF620296) by 16S rRNA gene sequence analysis by Dongsheng Wang of the College of Natural Resources and Environment, Northwest A&F University, Shaanxi Province, China.³¹ The strain was deposited in the Department of Resources Science, College of Natural Resources and Environment, Northwest A&F University, China.

Fermentation, Extraction, and Isolation. *S. cacaoi* subsp. *asoensis* H2S5 was preserved in 25% glycerol–water at −80 °C. A 50 mL Eppendorf tube containing 15 mL of medium (tryptone 15 g/L, peptone 5 g/L, NaCl 5 g/L, and an appropriate volume of MilliQ water, pH 7.0–7.4) was inoculated from a tube of H2S5 at 28 °C for 3 days with shaking at 130 rpm. Using aseptic technique, a portion of the spore suspension was transferred to a 250 mL Erlenmeyer flask containing 100 mL of seed medium and shaken at 130 rpm, 28 °C, for 3 days. An aliquot of the preculture (10 mL) was transferred into a 500 mL flask containing 200 mL of medium and incubated for 7 days at 28 °C with shaking at 130 rpm. Both the seed and production medium consisted of soluble starch 10 g/L, peptone 2 g/L, yeast extract powder 4 g/L, and NaCl 5 g/L; pH 7.0–7.4. All media were sterilized for 20 min at 121 °C in a steam autoclave.

After scale-up fermentation, the culture broth (70 L) was filtered to afford the supernatant and the mycelia. The supernatant was concentrated to 5 L by evaporation under reduced pressure, then extracted with ethyl acetate five times and with petroleum ether three times to remove small polar compounds. After suspending the extract

in MeOH–acetone (3:1 v/v) to disrupt cells, mycelia were extracted with petroleum ether and ethyl acetate. The EtOAc layers of the mycelium and filtrate were concentrated under reduced pressure to give a crude extract (16.8 g), which was applied to an RP-18 column and eluted with a gradient of MeOH–H₂O (10–100%) to yield 16 fractions, A–P. Fractions J (2.888 g), K (679.3 mg), and M (488.9 mg), which showed a series of peaks with 271 nm UV absorption by HPLC, were separated on a Sephadex LH-20 column in MeOH, affording Fr. J1–J9, Fr. K1–K6, and Fr. M1–M4, respectively.

Fr. J2 (2.5496 g) was separated on HSCCC with a two-phase solvent system composed of *n*-hexane–ethyl acetate–methanol–water (HEMWat, 4:6:4:6 v/v) four times, yielding **4** (Fr. J2.14, 106.1 mg), **8** (Fr. J2.17, 17 mg), and another 24 fractions. Fr. J2.7, J2.11, and J2.18–J2.26 were further purified by semipreparative HPLC to afford **5** (62%, MeOH–H₂O, 2 mL/min, *t*_R = 41.0 min, 51.1 mg), **6** (62%, MeOH–H₂O, 2 mL/min, *t*_R = 39.5 min, 10.6 mg), **10** (58%, MeOH–H₂O, 2 mL/min, *t*_R = 12.0 min, 3.6 mg), **9** (58%, MeOH–H₂O, 2 mL/min, *t*_R = 29.0 min, 6.7 mg), **2** (58%, MeOH–H₂O, 2 mL/min, *t*_R = 31.5 min, 1.3 mg), and **7** (60%, MeOH–H₂O, 2 mL/min, *t*_R = 40.7 min, 2.1 mg).

HSCCC also carried out to separate Fr. K2 (391.3 mg) with a two-phase solvent system composed of HE MWat (3:7:4:6 v/v), giving 13 fractions, K2.1–K2.13. Purification of Fr. K2.1 and Fr. K2.3 by HPLC provided **3** (68%, MeOH–H₂O, 2 mL/min, *t*_R = 34.8 min, 1.8 mg) and **1** (65%, MeOH–H₂O, 2 mL/min, *t*_R = 41.5 min, 15.5 mg).

Trienomycin J (1): white powder; $[\alpha]_D^{20} +118.8$ (*c* 0.25, MeOH); UV (MeOH) λ_{\max} (log ϵ) 250 (4.44), 260 (4.44), 271 (4.48), 282 (4.40) nm; IR (KBr) ν_{\max} 3320, 2930, 1715, 1654, 1547, 1370, 1217, 1000, 645 cm⁻¹; ¹H NMR (500 MHz) and ¹³C NMR (125 MHz) data (CD₃OD), see Table 1; positive ion HRESIMS *m/z* 647.3676 [M + Na]⁺ (calcd for C₃₆H₅₂N₂O₇Na, 647.3672).

Trienomycin K (2): white powder; $[\alpha]_D^{20} +105.2$ (*c* 0.25, MeOH); UV (MeOH) λ_{\max} (log ϵ) 250 (4.25), 260 (4.26), 271 (4.34), 282 (4.24) nm; IR (KBr) ν_{\max} 3297, 2972, 2314, 1723, 1656, 1545, 1212, 1091, 684 cm⁻¹; ¹H NMR (500 MHz) and ¹³C NMR (125 MHz) data (CD₃OD), see Table 1; positive ion HRESIMS *m/z* 605.3202 [M + Na]⁺ (calcd for C₃₃H₄₆N₂O₇Na, 605.3203).

Trienomycin L (3): white powder; $[\alpha]_D^{20} +130.0$ (*c* 0.20, MeOH); UV (MeOH) λ_{\max} (log ϵ) 250 (4.16), 260 (4.17), 271 (4.25), 282 (4.14) nm; IR (KBr) ν_{\max} 3432, 2929, 1718, 1651, 1544, 1210, 1002, 645 cm⁻¹; ¹H NMR (500 MHz) and ¹³C NMR (125 MHz) data (CD₃OD), see Table 1; positive ion HRESIMS *m/z* 619.3353 [M + Na]⁺ (calcd for C₃₄H₄₈N₂O₇Na, 619.3359).

Marfey's Analysis. Compound **4** (3.2 mg) was hydrolyzed in 6 N HCl (500 μ L) at 120 °C for 16 h. After completion of the reaction, the solvent was removed under vacuum. The dried residue was resuspended in water (100 μ L). Next 40 μ L of 1 M sodium bicarbonate and 100 μ L of 25 mM L-FDLA in acetone were added, and the mixture was incubated at 37 °C for 1 h. To neutralize the reaction, 40 μ L of 2 N HCl was added to the reaction mixture. The standard L- and D-alanine standards were derivatized separately. The crude product and the standard amino acids were diluted with 720 μ L of methanol, and 2 μ L of the solutions was subjected to HPLC analysis. HPLC was performed using an Agilent 1100 system. Separations were carried out on a YMC C₁₈ column (4.6 \times 150 mm; 5 μ m) at 30 °C using the following gradient elution program: solvent A, H₂O (0.1% formic acid); solvent B, methanol; 5–60% B from 0 to 5 min, 60–90% B from 5 to 25 min, 90–100% B from 25 to 26 min, and hold at 100% solvent B for 4 min. The flow rate was 0.8 mL/min with detection at 338 nm. The retention time data for the FDLA derivatives of the hydrolysate and the alanine standard are summarized in Table S1 (Supporting Information).

Preparation of an Acetonide Derivative of 4. Compound **4** (24 mg) was dissolved in tetrahydrofuran (789 μ L) and cooled to –23 °C. A solution of lithium aluminium hydride (1.0 M in Et₂O, 550 μ L) was added drop by drop. The reaction mixture was stirred at –23 °C for 1 h. After completion of the reaction, ethyl acetate (658 μ L) was added and the solution was washed with phosphate buffer (pH 7, 1316 μ L). The organic phase was separated, and the aqueous phase was extracted with ether (1316 μ L) three times. The combined

organic extracts were dried with anhydrous Na₂SO₄ and filtered, and the solvent was removed under reduced pressure. The crude product was dissolved in 658 μ L of 2,2-dimethoxypropane and 132 μ L of acetone, to which camphorsulfonic acid (0.263 mg) was added. The mixture was stirred at 25 °C for 2 h, and the reaction was quenched by addition of 132 μ L of triethylamine. The reaction mixture was further purified by semipreparative HPLC to afford compound **11** (82%, MeOH–H₂O, 2 mL/min, *t*_R = 21.3 min, 15.6 mg, 65% yield) as a colorless powder: $[\alpha]_D^{24} +140$ (*c* 0.21, CHCl₃); IR (CHCl₃) 3271, 3110, 2926, 2875, 1622, 1563, 1499, 1434, 1372, 1306, 1216, 1145, 1077, 1000 cm⁻¹; negative ion HRESIMS *m/z* 480.2739 [M – H][–] (calcd for C₂₉H₃₈NO₅, 480.2744); ¹H NMR (500 MHz, CDCl₃) δ_{H} 8.19 (s, 1H), 7.85 (s, 1H), 7.31 (s, 1H), 6.51 (s, 1H), 6.15–6.26 (m, 3H), 6.03–6.08 (m, 2H), 5.80–5.86 (m, 1H), 5.63 (dd, *J* = 15.0, 8.0 Hz, 1H), 5.24 (br apparent t, *J* = 6.5 Hz, 1H), 4.58 (d, *J* = 5.5 Hz, 1H), 4.03 (br apparent t, *J* = 10.6 Hz, 1H), 3.52 (m, 1H), 3.34 (s, 3H), 2.90 (dd, *J* = 13.0, 2.5 Hz, 1H), 2.44–2.57 (m, 4H), 2.08–2.16 (m, 3H), 1.89 (m, 1H), 1.73 (s, 3H), 1.35 (s, 3H), 1.30 (s, 3H), 0.82 (d, *J* = 7.0 Hz, 3H); ¹³C NMR (125 MHz, CDCl₃) δ_{C} 169.0, 157.7, 144.5, 138.1, 135.3, 135.2, 134.9, 133.5, 132.3, 131.6, 129.0, 125.3, 112.5, 109.7, 106.0, 100.8, 79.6, 73.3, 68.6, 56.6, 45.2, 37.1, 36.3, 36.1, 29.6, 24.8, 24.0, 20.4, 12.7.

Cytotoxicity Assay. The *in vitro* evaluation of the cytotoxicity of the pure compounds was performed in PC-3 prostate cancer cells and HepG2 cells by the SRB colorimetric assay with doxorubicin as the positive control and 0.1% DMSO as the negative control. IC₅₀ values were determined from dose–response curves using Origin 8 software. Briefly, 100 μ L aliquots (2.5 \times 10⁴ cells/mL) of exponentially growing cells were added to each well of a 96-well flat microtiter plate and allowed to attach. Next, the medium was replaced with fresh medium, and cells were incubated with various concentrations of the test compounds at 37 °C for 72 h. Four replicate wells were used per time point. Next, medium was decanted, and cells were fixed *in situ* with 100 μ L aliquots of cold 10% trichloroacetic acid and incubated for 1 h at 4 °C. Thereafter, supernatant was discarded, and the plates were washed five times with distilled water and air-dried. SRB solution at 0.4% (w/v) in 1% acetic acid was added to each well, and the plates were incubated for 20–30 min at room temperature. The unbound dye was removed by washing five times with 1% acetic acid and the plates were air-dried. Bound SRB was subsequently solubilized with 10 mM Tris base, and the absorbance at 560 nm was read using an Epoch (Bio-Tek) microplate reader. Percentage cell viability was calculated relative to control wells (designated 100% viable).

Hoechst Staining. The nuclear morphological changes of HepG2 cells exposed to **1** were evaluated using Hoechst 33342 staining. To this end, 1 \times 10⁶ cells were seeded on a coverslip in a six-well plate, treated with 1.0, 5.0, or 10 μ M **1**, respectively, for 48 h, and fixed for 30 min with 4% paraformaldehyde. The fixed cells were stained with Hoechst 33342 for 10 min at room temperature in the dark. The cells were subsequently washed with phosphate-buffered saline (PBS) and mounted on a slide for fluorescence microscopy.

Analysis of Apoptosis and the Cell Cycle. Apoptosis and the cell-cycle distribution were analyzed by flow cytometry.³² After treatment with DMSO and 0.5, 1.0, or 5.0 μ M **1** for 48 h, HepG2 cells were collected, washed in cold PBS, and resuspended in annexin V binding buffer. Annexin V–FITC was added, the mixture was incubated in the dark at 37 °C for 5 min, and PI was added before submitting to flow cytometry for apoptosis analysis. The cell-cycle distribution was also analyzed. HepG2 cells were treated with DMSO and 0.5, 1.0, and 5.0 μ M **1** for 24 h, washed in cold PBS, fixed by dropwise addition to ice-cold 95% ethanol, stored at 4 °C for at least 2 h, incubated with PI for 30 min at 37 °C, and subjected to a flow cytometer for cell-cycle distribution analysis.

Nitric Oxide Production Inhibitory Assays. BV-2 murine microglial cells were obtained from Peking Union Medical College Cell Bank (Beijing, China) and maintained in Dulbecco's modified Eagle's medium (DMEM) supplemented with 10% (v/v) heat-inactivated fetal bovine serum, penicillin (100 U/mL), and streptomycin (100 U/mL) at 37 °C with 5% CO₂. During logarithmic growth phase, BV-2 cells (2 \times 10⁴ /well) were seeded in 96-well

plates and incubated at 37 °C for 24 h. Next, the cells were treated with the test compounds at five concentrations for 24 h in DMEM with 1 µg/mL LPS (*Escherichia coli* 0111:B4, Sigma, MO, USA). LPS and DMSO were used as the controls.

The NO concentration in the medium was measured using a commercial assay kit, according to the protocol²⁴ with sodium nitrite as a standard. NO production was evaluated by quantifying nitrite in culture supernatants using the Griess reaction. Briefly, the culture supernatant of BV-2 cells (50 µL) was reacted with 50 µL of Griess reagent I in a 96-well plate. Subsequently, 50 µL of Griess reagent II was added to each well. The absorbance at 540 nm of the mixture was measured using a microplate reader. A nitrite standard curve was generated using the sodium nitrite standard. IC₅₀ values were calculated as the concentrations that reduced NO production by 50%. Quercetin was taken as the positive control.

Cell viability was evaluated by the MTT assay. BV-2 cells were seeded into 96-well plates at 2 × 10³ cells/100 µL of medium and incubated for 24 h. Next, the cells were incubated with trienomyocins at various concentrations and LPS for a further 24 h. Cells treated with DMSO alone were used as the negative control. Subsequently, 10 µL of MTT (5 mg/mL) was added, the plates were incubated at 37 °C for 4 h, and extraction buffer (100 µL, 10% sodium dodecyl sulfate, 5% isobutanol, and 0.1% HCl) was added to each well. After overnight incubation, the absorbance at 570 nm was measured using a microplate reader.

Molecular-Docking Studies. Molecular-docking simulations were performed using Autodock 4.2 Vina software and AutoDock Tools (ADT 1.5.6) using the hybrid Lamarckian Genetic Algorithm (LGA) as reported previously.³³ The three-dimensional (3D) crystal structure of iNOS (PDB code, 3E7G) was obtained from the RCSB Protein Data Bank. The standard 3D structures (PDB format) of the 10 compounds were constructed using the “SKETCH” option function in SYBYL-X, and a cubic grid box of 50 × 60 × 50 Å (*x*, *y*, *z*) with a spacing of 0.375 Å and grid maps were generated. The docking parameters were as follows: population size 150, number of evaluations 2 500 000, number of generations 270 000, number of top individuals that automatically survive 20, and number of docking runs 40; the default values of the other settings were used.

■ ASSOCIATED CONTENT

● Supporting Information

The Supporting Information is available free of charge on the ACS Publications website at DOI: 10.1021/acs.jnatprod.8b00203.

Additional information (PDF)

■ AUTHOR INFORMATION

Corresponding Author

*Tel: 86-29-87092335. E-mail: jinminggao@nwsuaf.edu.cn.

ORCID

Ling-Li Liu: 0000-0003-2081-4493

Jin-Ming Gao: 0000-0003-4801-6514

Author Contributions

[†]D. Tang and L.-L. Liu contributed equally to this work.

Notes

The authors declare no competing financial interest.

■ ACKNOWLEDGMENTS

This work was cofinanced by the National Natural Science Foundation of China (21602177, 21877089), the Natural Science and Basic Research Plan of Shaanxi Province (No. 2014JZ2-001), and the Fundamental Research Funds for the Central Universities (2452017176). The authors would like to thank Prof. Q. Xue for the actinomycetes material, Dr. Z. Yang from Northwest A&F University for the HSCCC analysis, and

N. Li from Life Science Research Core Services (LSRCS) at Northwest A&F University for the HRESIMS data.

■ REFERENCES

- (1) Komiyama, K.; Hirokawa, Y.; Yamaguchi, H.; Funayama, S.; Masuda, K.; Anraku, Y.; Umezawa, I.; Omura, S. *J. Antibiot.* **1987**, *40*, 1768–1772.
- (2) Lu, C.; Li, Y.; Deng, J.; Li, S.; Shen, Y.; Wang, H.; Shen, Y. *J. Nat. Prod.* **2013**, *76*, 2175–2179.
- (3) Umezawa, I.; Funayama, S.; Okada, K.; Iwasaki, K.; Satoh, J.; Masuda, K.; Komiyama, K. *J. Antibiot.* **1985**, *38*, 699–705.
- (4) Qu, X.; Lei, C.; Liu, W. *Angew. Chem., Int. Ed.* **2011**, *50*, 9651–9654.
- (5) Kang, Q.; Shen, Y.; Bai, L. *Nat. Prod. Rep.* **2012**, *29*, 243–263.
- (6) Funayama, S.; Cordell, G. A. *Stud. Nat. Prod. Chem.* **2000**, *23*, 51–106.
- (7) Sensi, P. *Clin. Infect. Dis.* **1983**, *5S*, S402–S406.
- (8) Funayama, S.; Okada, K.; Iwasaki, K.; Komiyama, K.; Umezawa, I. *J. Antibiot.* **1985**, *38*, 1677–1683.
- (9) Nomoto, H.; Katsumata, S.; Takahashi, K.; Funayama, S.; Komiyama, K.; Umezawa, I.; Omura, S. *J. Antibiot.* **1989**, *42*, 479–481.
- (10) Smith, A. B.; Wood, J. L.; Gould, A. E.; Omura, S.; Komiyama, K. *Tetrahedron Lett.* **1991**, *32*, 1627–1630.
- (11) Kim, W. G.; Song, N. K.; Yoo, I. D. *J. Antibiot.* **2002**, *55*, 204–207.
- (12) Kawamura, T.; Tashiro, E.; Yamamoto, K.; Shindo, K.; Imoto, M. *J. Antibiot.* **2008**, *61*, 303–311.
- (13) Song, Y. N.; Jiao, R. H.; Zhang, W. J.; Zhao, G. Y.; Dou, H.; Jiang, R.; Zhang, A. H.; Hou, Y. Y.; Bi, S. F.; Ge, H. M.; Tan, R. X. *Org. Lett.* **2015**, *17*, 556–559.
- (14) Song, Y. N.; Zhang, W. J.; Bi, S. F.; Jiao, R. H.; Tan, R. X.; Ge, H. M. *J. Antibiot.* **2015**, *68*, 757–759.
- (15) Funayama, S.; Anraku, Y.; Mita, A.; Yang, Z. B.; Shibata, K.; Komiyama, K.; Umezawa, I.; Omura, S. *J. Antibiot.* **1988**, *41*, 1223–1230.
- (16) Brandt, G. E. L.; Blagg, B. S. J. *ACS Med. Chem. Lett.* **2011**, *2*, 735–740.
- (17) Del Valle, D. J.; Krische, M. J. *J. Am. Chem. Soc.* **2013**, *135*, 10986–10989.
- (18) Smith, A. B.; Wan, Z. H. *J. Org. Chem.* **2000**, *65*, 3738–3753.
- (19) Chen, S.; von Bamberg, D.; Hale, V.; Breuer, M.; Hardt, B.; Muller, R.; Floss, H. G.; Reynolds, K. A.; Leistner, E. *Eur. J. Biochem.* **1999**, *261*, 98–107.
- (20) Li, X.; Zhu, J.; Shi, G.; Sun, M.; Guo, Z.; Wang, H.; Lu, C.; Shen, Y. *RSC Adv.* **2016**, *6*, 88571–88579.
- (21) Bai, R.; Zhang, C. C.; Yin, X.; Wei, J.; Gao, J. M. *J. Nat. Prod.* **2015**, *78*, 783–788.
- (22) (a) Gao, J. M.; Yang, S. X.; Qin, J. C. *Chem. Rev.* **2013**, *113*, 4755–4811. (b) Xiao, J.; Zhang, Q.; Gao, Y. Q.; Tang, J. J.; Zhang, A. L.; Gao, J. M. *J. Agric. Food Chem.* **2014**, *62*, 3584–3590.
- (23) (a) Wei, J.; Liu, L. L.; Dong, S.; Li, H.; Tang, D.; Zhang, Q.; Xue, Q. H.; Gao, J. M. *Bioorg. Med. Chem. Lett.* **2016**, *26*, 4903–4906. (b) Wei, J.; Zhang, X. Y.; Deng, S.; Cao, L.; Xue, Q. H.; Gao, J. M. *Nat. Prod. Res.* **2017**, *31*, 2062–2066.
- (24) (a) Wei, J.; Cheng, Y.; Guo, W. H.; Wang, D. C.; Zhang, Q.; Li, D.; Rong, J.; Gao, J. M. *Sci. Rep.* **2017**, *7*, 8883. (b) Wei, J.; Guo, W. H.; Cao, C. Y.; Kou, R. W.; Xu, Y. Z.; Górecki, M.; Di Bari, L.; Pescitelli, G.; Gao, J. M. *Sci. Rep.* **2018**, *8*, 2175.
- (25) Li, R.; Zhu, H.; Ruan, J.; Qian, W.; Fang, X.; Shi, Z.; Li, Y.; Li, S.; Shan, G.; Kristiansen, K.; Li, S.; Yang, H.; Wang, J.; Wang, J. *Genome Res.* **2010**, *20*, 265–272.
- (26) Li, R.; Li, Y.; Kristiansen, K.; Wang, J. *Bioinformatics* **2008**, *24*, 713–714.
- (27) Blin, K.; Medema, M. H.; Kottmann, R.; Lee, S. Y.; Weber, T. *Nucleic Acids Res.* **2017**, *45*, D555–D559.
- (28) Smith, A. B.; Wood, J. L.; Wong, W.; Gould, A. E.; Rizzo, C. J.; Barbosa, J.; Komiyama, K.; Omura, S. *J. Am. Chem. Soc.* **1996**, *118*, 8308–8315.

- (29) Marfey, P. *Carlsberg Res. Commun.* **1984**, *49*, 591–596.
- (30) Skehan, P.; Storeng, R.; Scudiero, D.; Monks, A.; McMahon, J.; Vistica, D.; Warren, J. T.; Bokesch, Kenney, H. S.; Boyd, M. R. *J. Natl. Cancer Inst.* **1990**, *82*, 1107–1112.
- (31) Wang, D. S. Study of microbial flora and antagonistic actinomycete resources in five habitats on north side of Taibai Mountain, the main peak of Qin Mountains. Ph.D. Thesis, Northwest A & F University, 2014; p 88.
- (32) Tang, J. J.; Dong, S.; Han, Y. Y.; Lei, M.; Gao, J. M. *MedChemComm* **2014**, *5*, 1584–1589.
- (33) Li, D.; Chi, B.; Wang, W. W.; Gao, J. M.; Wan, J. *Med. Chem. Res.* **2017**, *26*, 153–169.